Ocean Dynamics (2014) 64:809–822
DOI 10.1007/s10236-014-0716-7

Role of fronts in the formation of Arabian Sea barrier layers during summer monsoon

Clément de Boyer Montégut · Fabien Durand · Romain Bourdallé-Badie · Bruno Blanke

Received: 14 January 2014 / Accepted: 28 March 2014 / Published online: 3 May 2014

Abstract The barrier layer (BL) — a salinity stratification embedded in the upper warm layer — is a common feature of the tropical oceans. In the northern Indian Ocean, it has the potential to significantly alter the air–sea interactions. In the present paper, we investigate the spatio-temporal structure of BL in the Arabian Sea during summer monsoon. This season is indeed a key component of the Asian climate. Based on a comprehensive dataset of Conductivity–Temperature–Depth (CTD) and Argo in situ hydrographic profiles, we find that a BL exists in the central Arabian Sea during summer. However, it is highly heterogeneous in space, and intermittent, with scales of about ~100 km or less and a couple of weeks. The BL patterns appear to be closely associated to the salinity front separating two water masses (Arabian Sea High Salinity Water in the Northern and Eastern part of the basin, fresher Bay of Bengal Water to the south and to the west). An ocean general circulation model is used to infer the formation mechanism of the BL. It appears that thick (more than 40 m) BL patterns are formed at the salinity front by subduction of the saltier water mass under the fresher one in an area of relatively uniform temperature. Those thick BL events, with variable position and timing, result in a broader envelope of thinner BL in climatological conditions. However, the individual patterns of BL are probably too much short-lived to significantly affect the monsoonal air–sea interactions.

Keywords Barrier layer · Arabian Sea · Summer monsoon · ARGO · ASHSW

Responsible Editor: Eric Deleersnijder

Electronic supplementary material The online version of this article (doi:10.1007/s10236-014-0716-7) contains supplementary material, which is available to authorized users.

C. de Boyer Montégut (✉)
IFREMER, Centre de Brest, Laboratoire d'Océanographie Spatiale, Pointe du Diable, B.P. 70, 29280 Plouzané, France
e-mail: deboyer@ifremer.fr

F. Durand
IRD, LEGOS, UMR5566 CNRS–CNES–IRD–UPS, 14 Avenue Edouard Belin, 31400 Toulouse, France
e-mail: fabien.durand@ird.fr

R. Bourdallé-Badie
Mercator Océan, 8-10 rue Hermes, Parc Technologique du Canal, 31520 Ramonville Saint-Agne, France
e-mail: rbourdal@mercator-ocean.fr

B. Blanke
Laboratoire de Physique des Océans, UMR 6523 CNRS-IFREMER-IRD-UBO, CNRS, Brest, France
e-mail: blanke@univ-brest.fr

1 Introduction

The tropical oceans frequently present a peculiar thermohaline stratification in the upper part of the water column, known as the barrier layer (BL) (Lukas and Lindstrom 1991). It consists of a salt-stratified, stable layer embedded within the warm, upper layer of the ocean. It was termed BL because it opposes the vertical exchanges of heat between the upper mixed layer (ML) and the underlying cooler thermocline. Figure 1 exemplifies this feature in the Arabian Sea. In the absence of BL, when turbulence is high enough in the ML, cooler thermocline water is mixed and/or entrained in the ML, reducing the ML temperature. The presence of a BL completely changes this picture: the ML water can only mix with and/or entrain BL water, which is as warm or even warmer (see de Boyer Montégut et al. 2007a for a map of temperature inversions below the ML): ML water does not cool through vertical exchanges. This is known to play an important climatic role in various regions of the tropics, such as the western Pacific Ocean for El Niño initiation (Maes et al. 2005), or in the

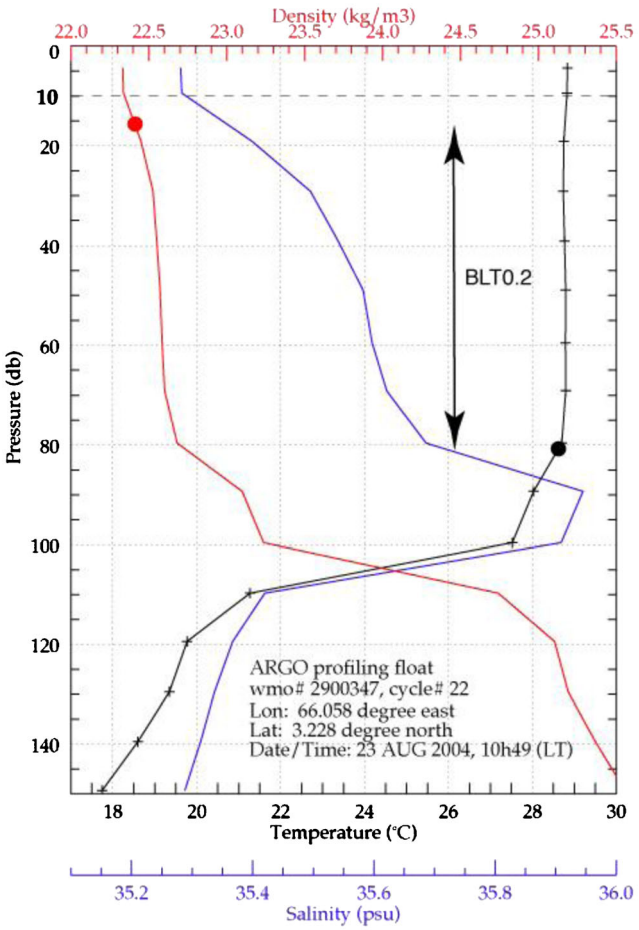

Fig. 1 Example of a barrier layer (*BL*) occurrence in the upper layer of the ocean: hydrographic profiles observed by ARGO float #2900347 in the study area (66.058°E, 3.228°N) during the 2004 summer monsoon. Temperature (resp. salinity, density) is in *black* (resp. *blue*, *red*). The *black bullet* shows the depth where the temperature is 0.2 °C colder than at 10 m (T10). The red bullet shows the depth of the equivalent density increase, it represents the mixed layer depth (MLDρ, see text). The dashed line indicates the surface reference level at 10 m depth. The BL thickness in the sense of T10-0.2 °C, named BLT0.2, is defined as the depth difference between the black and red bullets. Here, we have BLT0.2=65 m

South-eastern Arabian Sea for Indian monsoon onset (Masson et al. 2005). The western Pacific warm pool and the South-eastern Arabian Sea are indeed regions where the BL is a robust feature, throughout the year or in some seasons only (Mignot et al. 2007). The BL forms under various possible mechanisms. Cronin and McPhaden (2002) describe four types of processes by which a BL can form and/or grow (see their Fig. 1). First, a BL can be advected from one region to another through horizontal advection. Second, a BL can grow or decay through vertical stretching of the water column. The two mechanisms both require a pre-existing BL to occur and will not create "new" BL conditions by themselves. Third, rainfall can cause a new BL to form between the base of the newly formed fresh lens and the top of the thermocline. Last, the "tilting" mechanism forms a barrier layer when a vertically sheared horizontal flow advects a horizontal salinity gradient within the isothermal surface layer. This causes near-vertical salinity contours to tilt along the horizontal, thus generating a shallow halocline above the top of the thermocline. An important point raised by Cronin and McPhaden (2002) is that "when analysing the formation of barrier layers, one must consider not only processes governing salinity stratification, but also how they occur without generating a corresponding temperature stratification." This is especially true for the tilting mechanism, which requires both a shear component in the horizontal direction across the salinity horizontal gradient and a relatively smaller temperature horizontal gradient (as regards to density variations) in the same direction.

The tilting mechanism appears as a singular process, in that it does not require the pre-existence of a BL, nor any atmospheric freshwater supply. Durand et al. (2007) demonstrated that the latter mechanism is basically responsible for the thick BL observed in the South-eastern Arabian Sea in winter. More controversial is the BL reported by Rao and Sivakumar (2003; henceforth RS03) and by Thadathil et al. (2008; henceforth T08) in the South Central Arabian Sea (SCAS) during summer monsoon. These authors suggested that a thick (20–60 m) BL forms there in June, and survives until September, over an extended area. To explain its formation, T08 proposed a mechanism amounting to tilting, consisting of a large-scale foliation of low-salinity water of equatorial origin at the surface, blanketing Arabian Sea High Salinity Water (ASHSW; Prasanna Kumar and Prasad 1999; Prasad and Ikeda 2002) at subsurface. This conclusion stands in contrast with that of Mignot et al. (2009; henceforth M09) and of Agarwal et al. (2012; henceforth A12). Indeed, based on different observational datasets and/or gridding methodologies, these authors basically showed that limited BL patterns, from 5 to 20 m thick, are observed in the SCAS in summer. The area is known to present limited precipitation during summer monsoon (typically less than 200 mm over June–September to the west of 65°E; Hoyos and Webster 2007), which makes unlikely a local formation of the BL by the "rainfall" mechanism of Cronin and McPhaden (2002). It rather presents a deep ML during this season, owing to the vigorous Findlater jet that blows northeastward from June through October (de Boyer Montégut et al. 2007b). Such an energetic turbulent mixing does not favour a consistent, thick BL, lasting several months. M09 provided a quantification of the patchiness of the BL regarding some given space and time scales, under the form of a "porosity" parameter, called barrier layer porosity (BLP). For a given grid box (e.g., 2°×2°, 1 month), this is defined as the ratio of the number of non-existing or insignificant BL thickness (BLT) over the total number of profiles in the box. Thus, assuming we have enough profiles in the box and they are distributed rather homogeneously (see M09 for

details), it approximates the probability that the water column does not present any BL in a given spatio-temporal box. In our example (2°×2°, 1 month grid box), a porosity of 50 % is consistent with a BL lasting only half of the month or occurring only over half of the grid cell, or a mix of the two. Interestingly, their results show that the BL appearing in the SCAS during summer monsoon has a porosity of about 50 % (ranging from 25 % to 75 % for 2°×2°, monthly grid boxes). Hence, it may not be considered as a robust and durable feature regarding space-time scales of 1 month and 200 km.

The present study basically aims at reconciling the four contradictory studies of RS03, T08 on one hand, and M09 and A12 on the other hand. Specifically, we revisit the following issues: What is the observed seasonal evolution of the BL in the SCAS? What is its spatial structure? How does it vary from year to year? What is the mechanism that forms it? Has it a sufficient time and space extension to play any climatic role? To do so, we make use of in situ observations and of an ocean general circulation model.

The paper is organized as follows. Section 2 presents the dataset and the numerical model. Sections 3 and 4 quantitatively detail the observed and modeled BL, respectively. Section 5 investigates its formation mechanism. Section 6 concludes the study.

2 Data and methods

2.1 In situ data

In the present study, we use in situ profiles of temperature and salinity measurements coming from the Conductivity–Temperature–Depth (CTD) profiles of the World Ocean Database 2009 (WOD09; Boyer et al. 2009), and from the profiling floats of the Argo program. WOD09 covers the period 1974 to 2008 quite irregularly with more data around 1980 and in the 1990s. Argo floats data span the 2002–2012 period. For our study area, i.e., the Arabian Sea (40°E–85°E, 5°S–25°N), it makes a total of 41,496 pairs of T/S profiles (36,568 Argo profiles and 4,928 CTD profiles). Those data went through basic checks (depth and density inversion, outlier range, gradient check) and only Argo measurements with quality flags 1 ("good data") or 2 ("probably good data") were kept here. CTD vertical resolution is of order 2 m while Argo profiles vertical resolution is about 10 m or less in the upper 100 m. Regarding the latter, a BLT less than 5 m should thus be viewed with caution and considered as a situation where no significant BL exists (see grey shading in Fig. 2).

Our BLT criterion is based on a 0.2 °C threshold, following de Boyer Montégut et al. (2007a). The BLT is computed as the difference between the top of the thermocline depth (TTD; defined as the depth where temperature decreases by 0.2 °C compared to temperature at 10 m depth), and the ML depth in density, using the associated variable density criterion (MLDρ; defined as the depth where density increases by an amount corresponding to a 0.2 °C temperature decrease). The BLT is computed from individual profiles as in de Boyer Montégut et al. (2004), and we will mainly present here monthly binned fields at 1° resolution. The binning on the regular grid was done by picking the median BLT value of all individual observed profiles available in each grid cell.

2.2 Model

The model used in this work is the ORCA025 version of the NEMO (Nucleus for European Modelling of the Ocean) ocean general circulation model (OGCM) described by Madec (2008). The model solves the primitive equations on an Arakawa (1966) C-grid over the global ocean, with 0.25° horizontal resolution and 50 vertical levels on a z-grid. The vertical resolution varies with depth (viz. 1 m at the surface, 10 m at 50 m, 20 m at 100 m) in order to satisfactorily simulate the ML dynamics. The vertical physics is based on a prognostic equation for the turbulent kinetic energy (Blanke and Delecluse 1993). The lateral diffusion is computed along isopycnal levels, with a Laplacian parameterization (K_h=300 m^2 s^{-1}). The lateral viscosity is computed along horizontal levels with a bi-Laplacian operator (A_h=−1.5 10^{11} m^4 s^{-2}). Viscosity is enhanced within [2.5°S, 2.5°N] by adding a Laplacian parameterization with the viscosity coefficient reaching 200 m^2 s^{-1} at the equator. The model starts from a motionless state on 1st January 1999 with World Ocean Atlas 2005 (WOA05; Locarnini et al. 2006; Antonov et al. 2006) temperature and salinity fields and runs until end of 2006. In order to get rid of the model spinup phase, we consider the simulation over the 2002–2006 period only. The atmospheric boundary conditions consist of surface fluxes of momentum, heat, and freshwater. The momentum and precipitation fluxes are prescribed; all other fluxes (heat and evaporation) are diagnosed from specified atmospheric variables through the CLIO (Coupled Large-scale Ice–Ocean model) bulk formulae (Goosse et al. 2001). All atmospheric fields (including momentum and precipitation) are daily means computed from the ECMWF 6-hourly operational analysis (http://www.ecmwf.int/products/forecasts/guide/). The model sea surface salinity (SSS) is weakly restored to WOA05 climatology to prevent any long-term drift of SSS. The large-scale component of the precipitation flux is nudged towards Global Precipitation Climatology Project (GPCP; see http://precip.gsfc.nasa.gov/) monthly data within 30°N–30°S. The model simulation is stored as 3-day running means. The model set-up is very similar to the one used in Durand et al.

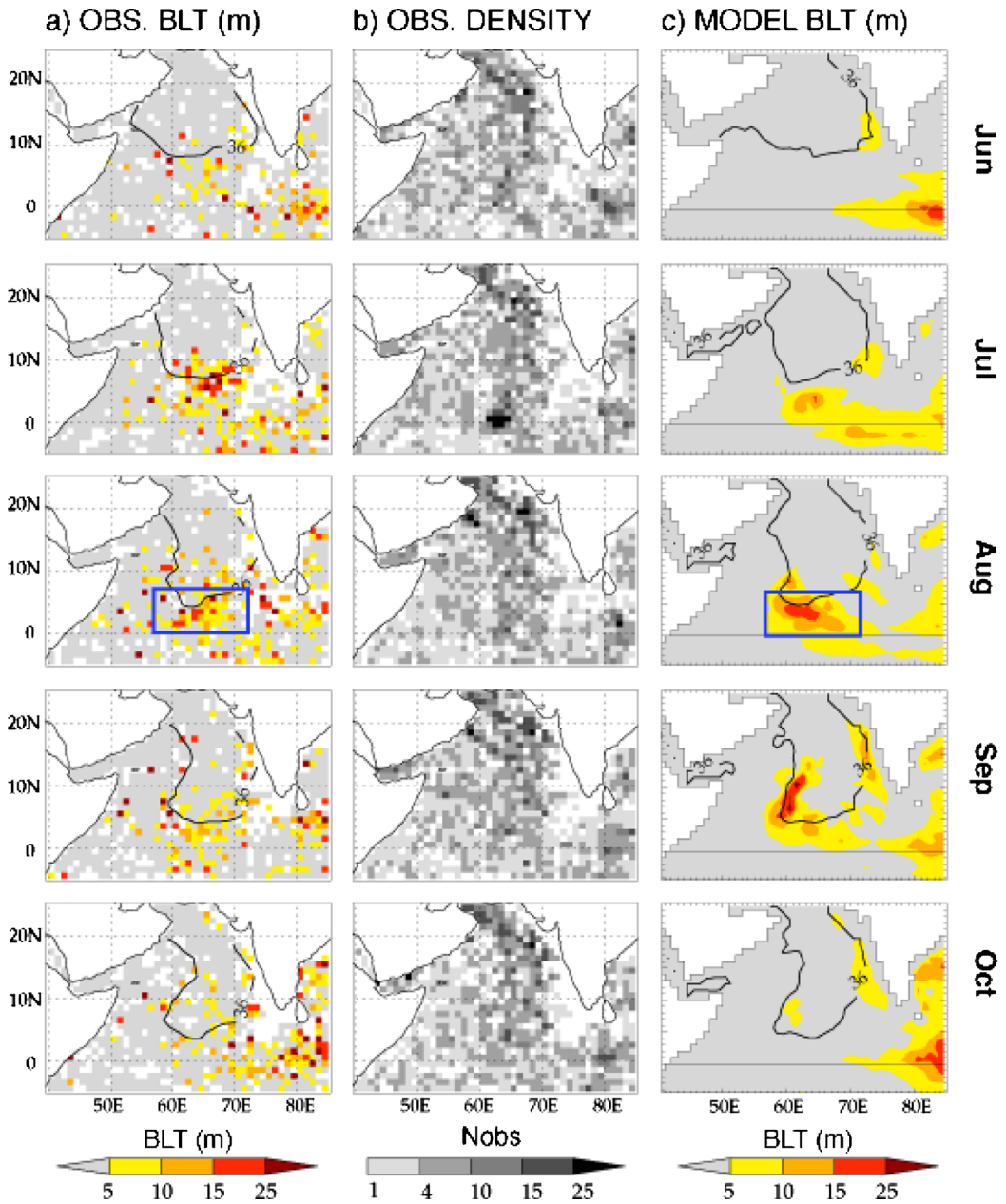

Fig. 2 **a** Monthly climatology of the observed BLT for the summer monsoon season. The month is indicated on the *right-hand side*. The frame in *blue* delimits the South Central Arabian Sea (*SCAS*) domain, used subsequently in this study. The 36 psu isoline at 70 m depth from Roemmich and Gilson dataset (2009), corresponding to the limit of the ASHSW (Prasad and Ikeda 2002), is also shown. **b** Corresponding distribution of the number of profiles per 1°×1° mesh box. **c** Same as **a** for the model simulation, and at 78 m depth for the 36 psu isoline

(2013). It was found to reproduce satisfactorily the seasonal cycle of temperature, salinity and currents in the Northern Indian Ocean (not shown; see Durand et al. (2013) and references therein for a complete validation of the model run). A specific validation of the seasonal cycle of the model SSS is provided as supplementary material (see Fig. S1). The BLT in the model outputs is based on the same criterion as for the observations. We will specifically validate this parameter in Section 4.

3 Observed structure of the BLT

3.1 Climatology

Figure 2a presents the monthly climatology of BLT from observations, from June to October. The BL builds up in the SCAS in June, peaks in July–August and decays afterwards. It disappears by October. Data coverage gives a good confidence in the observed evolution (Fig. 2b).

The BLT barely reaches 25 m locally in July–September, and only for a few grid cells. No broad, consistent area of large BLT appears (unlike what was seen for example in the South-eastern Arabian Sea in winter by Durand et al. 2007). To a certain extent, the isolated patches of large BLT that occur in the observations are associated with the presence of the subsurface 36 psu isohaline, which is known to be a good proxy for the limit of the ASHSW at about 70 m depth (Prasad and Ikeda 2002).

The average BLP in the observations at 2° resolution in August over the SCAS box (57°E–72°E; 0–7°N) is 50 %. This indicates that space and lifetime of the BL are of order 15 days and/or 100 km or less. For comparison, the South-eastern Arabian Sea in January shows a BLP lower than 10 % over an area of more than 5°×5°, thus showing a large region of permanent BL there.

3.2 Variability of the BLT

Figure 3 shows the detailed locations of individual (profile-wise) BLTs in observations for August in the SCAS, along with their distribution. The BL appears to be very patchy, with the occurrence of BL-free situations (grey bullets in Fig. 3) all over the area. The BLT distribution is skewed, with a maximum peak below 5 m. Those results echo the above-mentioned high BL porosity over our area (about 50 %). Consistently, half the distribution of BLT is below 5 m. BLTs reach values in excess of 50–60 m on some occasions but these events are quite rare.

4 Barrier layer simulated by the model

4.1 Climatology

Figure 2c presents the model monthly climatology of BLT computed over 2002–2006, with the resolution of the model downgraded to 1° to be consistent with the observational grid. The first point to notice is that the model simulates a BL in the Arabian Sea during the summer season, consistently with the observations. The BLT maximum modeled in the SCAS is located satisfactorily. Its seasonal evolution is also in line with the observations, with an initiation in June, a maximum reached in August, followed by a decay through October. Co-occurrence of thick BLT areas and of the ASHSW limit at subsurface (78 m depth) is also seen in the model. At this resolution (1°), the BLT hardly reaches 25 m on few occasions, just like in the observed field. When considering the native 0.25° resolution of the model, BLP also amounts to about 50 % over the SCAS. One exception is the small area of 200 km width centred on 64°E–2°N (maximum BLT in August) that shows BLP lower than 10 %, revealing a quasi-permanent BL there in the model. On average, significant BL events (in the sense: thicker than 5 m and thicker than 10 % of the TTD; see M09) occur twice in August, and last about 10 days each. Since the BLP is 50 % on the 0.25° grid, the order of magnitude for the BL space scale is about 20 km, using factors 2/3 in time (for 20 days of BL over the month, see above) and thus 3/4 in space. One must keep in mind that the spatial scales resolved by the model are very distinct from that resolved by the observed climatology. This is clearly seen in the remnant meso-scale patterns that show up in the model climatology, but cannot be resolved by the observational grid of 1°×1°.

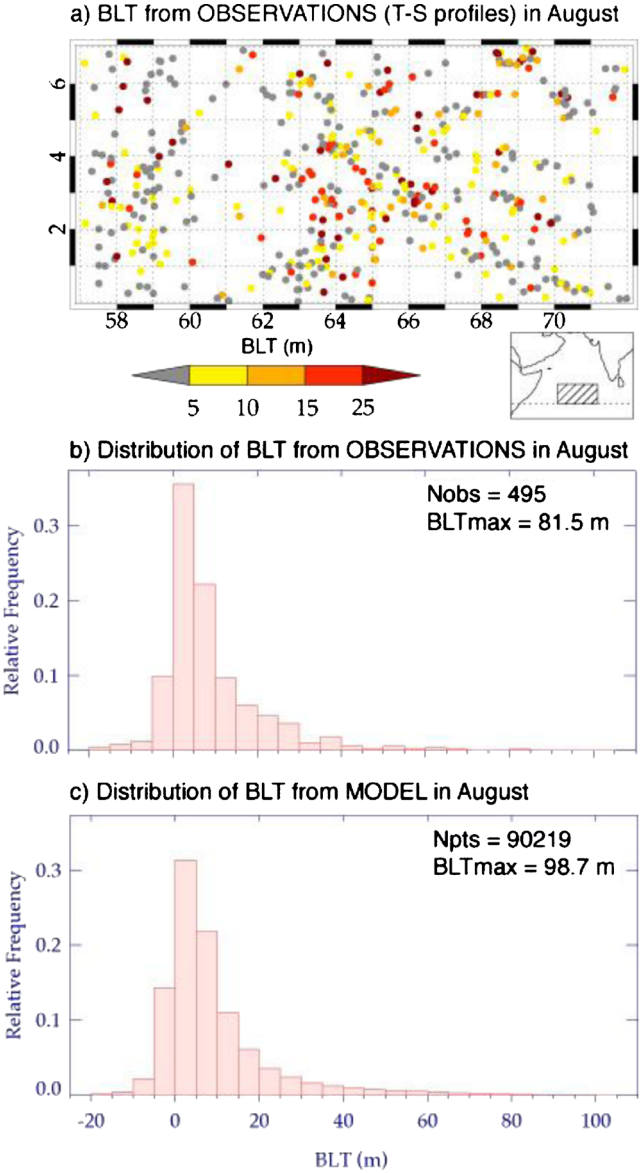

Fig. 3 **a** Map of observed BLT recorded for all the individual profiles falling in August over the SCAS domain. The full domain is shown as an insert. **b** Distribution of BLTs in August in the SCAS domain for the observations. **c** Same as **b** for the model

4.2 Year-to-year variability of the modeled BLT

Figure 3c shows the distribution of modeled BLT in August. Just like in the observed field, the distribution is skewed, with very limited number of BL events thicker than 50–60 m. Figure 4 presents the instantaneous structure of the BL simulated by the model at the exact date when BLT reaches its annual maximum in the Arabian Sea, during summer (from June to October), for each year from 2002 to 2006. Note that the timing of this maximum shows some year-to-year variability, from late July (in 2004) to mid September (in 2003). It is obvious that the BL in the SCAS never appears as an organized large-scale feature. Rather, it takes the form of elongated patterns, reminiscent of mesoscale fronts. The typical width of a given feature is about 100 km, with a typical length of a few hundreds of km. The orientation of the patterns is extremely variable, from north–south (on 1 September 2002) to east–west (on 31 July 2004). The simulated BLT is very large (in excess of 65 m in the core of the individual patterns) but confined in space. The gradients of BLT are thus

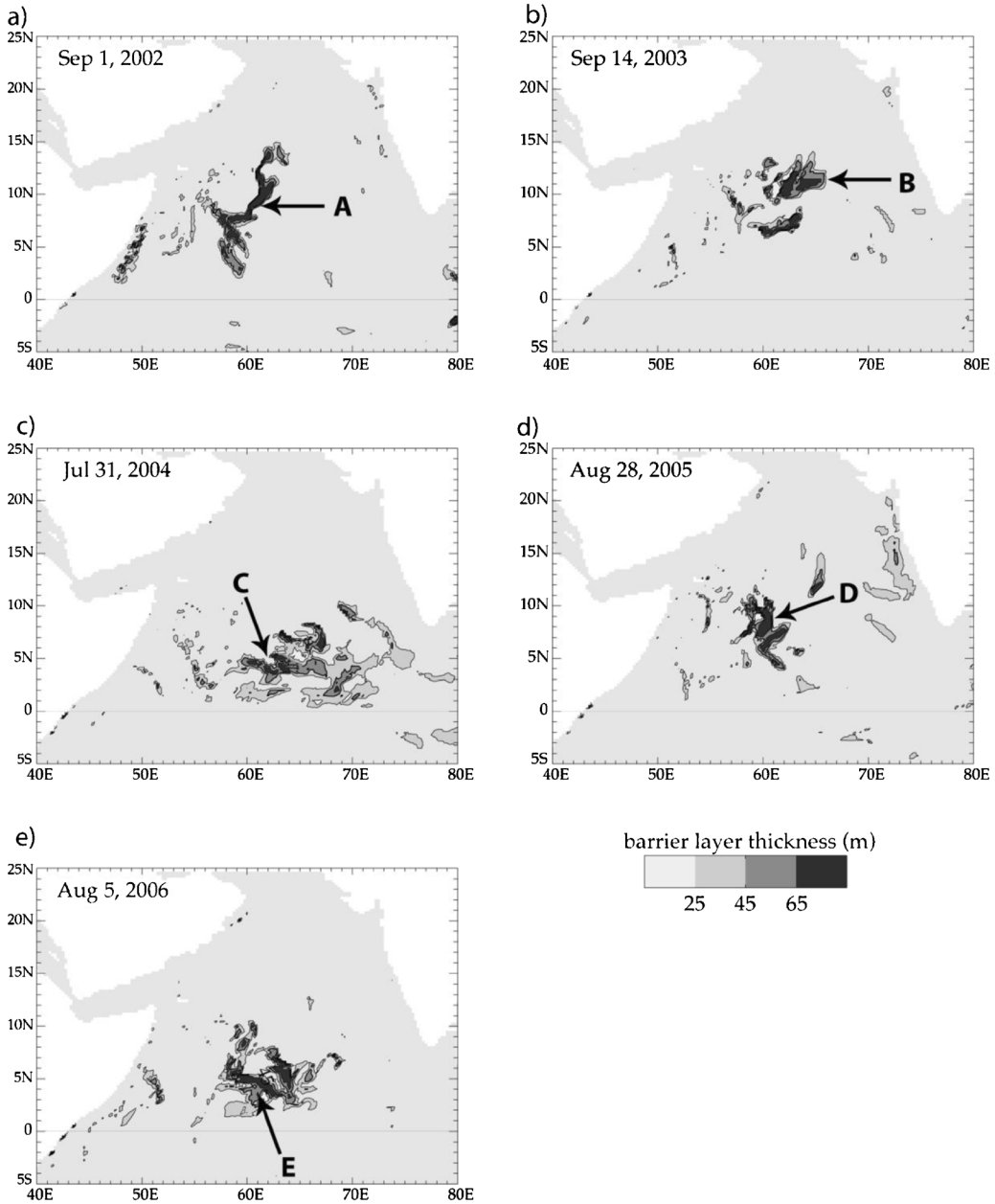

Fig. 4 BLT simulated by the model on selected dates, as indicated on each frame. The patterns indicated by *arrows* will be studied in detail. Isocontours are every 20 m

extremely marked, over scales close to the model grid spacing (0.25°). On each snapshot, one can typically see two patterns of thick BL, one close to the other. This stands in contrast with the smoother pattern seen on the monthly climatological evolution (Fig. 2c) and suggests that the climatological BL area seen in SCAS in summer should actually be considered as the geographical envelope of thicker, intermittent features, apparently distributed randomly within the SCAS.

5 Barrier-layer formation process

Figure 5 presents the instantaneous salinity field simulated at 78 m depth on the same dates as the occurrence of the yearly maximum BLT (shown in Fig. 4), for each year from 2002 to 2006. This depth was chosen because it corresponds to the typical depth of the core of the BL. As we already saw in the validation of the model (Section 2), it reproduces satisfactorily the two water masses that are known to co-exist in the Arabian Sea, with the ASHSW (salinity in excess of 36.2 psu; Prasad and Ikeda 2002) in the north-eastern quarter of the basin and the Bay of Bengal Water (BBW; salinity inferior to 35.8 psu; Tomczak 1999) occupying the rest of the basin. A frontal salinity zone, typically centred on 35.8–36.2 psu, separates the two water masses. This stands in very good agreement with the observed climatologies reported by Prasanna Kumar and Prasad (1999) or Chatterjee et al. (2012) (Fig. S1). Figure 5 also displays the positions of the grid points presenting an extremely thick BL at the time considered for plotting. These grid points are objectively defined by a threshold in BLT, conveniently chosen for each snapshot in order to isolate a few dozens of points (for a reason explained in the next paragraph). The value of the threshold as well as the resulting number of grid points is provided in Table 1. Interestingly, the patches of thick BL are concentrated in the frontal area and, in each of the presented snapshots, the pattern of thickest BL stretches exactly along an iso-haline featuring the salinity front. The three-dimensional structure of these patterns is investigated in Fig. 6. It presents vertical sections of temperature and salinity in the east–west (years 2002, 2003 and 2005) or north–south (years 2004 and 2006) direction. They are defined so as to cut through the salinity front in each area of maximal BLT. The frontal salinity structure allows to delineate the two water masses already introduced in the upper 100 m, with ASHSW corresponding to salinities in excess of 36.2 psu confined in the eastern (2002, 2003, 2005) or in the northern (2003, 2006) part of each section, and BBW on the other side. The salinity gradient is associated with a temperature gradient only for the 2002 and 2003 events. At the exact position of the maximum BLT, the profiles of temperature and salinity show that the model simulates a typical increase in salinity of about 0.15–0.2 psu between the surface and the core of the BL (in 2002, 2003, 2004 and 2005), reaching an extreme 0.5 psu in 2006. The BL typically lies between 20–50 and 100–130 m. A weak vertical temperature gradient exists from the surface down to the bottom of the BL. From these vertical sections, it becomes clear that the BL is associated with subsurface inflow of ASHSW, leaking below the BBW lying at the surface. Strikingly, the foliation of ASHSW below BBW occurs typically over a band 100–300 km wide only. In a nutshell, the model simulates small-scale BL patterns, intimately linked with the salinity front. This is consistent with what has been seen in the observations in Section 3. The detailed structure of the modeled BL is hard to validate extensively, given the limited space-time coverage of the available observations. However, on some occasions in situ data allow to confirm the picture inferred from the model outputs (see Fig. S2).

To understand more clearly the three-dimensional circulation leading to the formation of these BL structures in the SCAS, we make use of an offline Lagrangian trajectory analysis tool (Blanke and Raynaud 1997). This tool allows tracing the pathways of a given water mass, and provides its thermal and haline properties along the diagnosed streamlines (Blanke et al. 1999). We adopt an approach very similar to Durand et al. (2007) by tracing backward in time the pathway and salinity of the water mass eventually found in the core of each of the five BL patterns discussed in the previous paragraph. We do this by initializing Lagrangian synthetic particles at every grid point constituting the area of maximum BLT (the positions of the grid points are shown by triangles in Fig. 5 and their number is given in Table 1). We then trace their trajectories backward in time by integrating the 3-day model currents from the date of the maximum BLT (indicated in Figs. 4, 5, and 6). As expected from the time considerations given in Section 4.1, we found that for all the events, a 55-day integration is long enough to cover the BL formation phase. Figure 7 presents the result of the Lagrangian tracing, with the age, depth and salinity of the particles plotted along the streamlines. For every BL event from 2002 to 2006, the particles predominantly follow a southward route originating in the northwestern Arabian Sea. This roughly corresponds to the orientation of the salinity front shown in Fig. 5, for each year. Some of the particle batches (2002, 2004, 2005) exhibit an undulating trajectory, in line with the known presence of large anticyclonic eddies (Great Whirl, Socotra Gyre) in this part of the basin during summer monsoon and centred to the west of the region we analyse (e.g., Wirth et al. 2002; Esenkov et al. 2003). Almost all batches experience downwelling along their trajectory, from an initial depth of about 10–30 m to a final depth of about 60 m when they end up in the core of the BL. The only exception is the 2003 batch that experiences a quasi-horizontal displacement (i.e., with little depth variability along streamlines). In general, the salinity of the particles does not vary much along streamlines, in accordance with circulation pathways broadly parallel to the direction of the salinity front. Everything above suggests that the BL formation

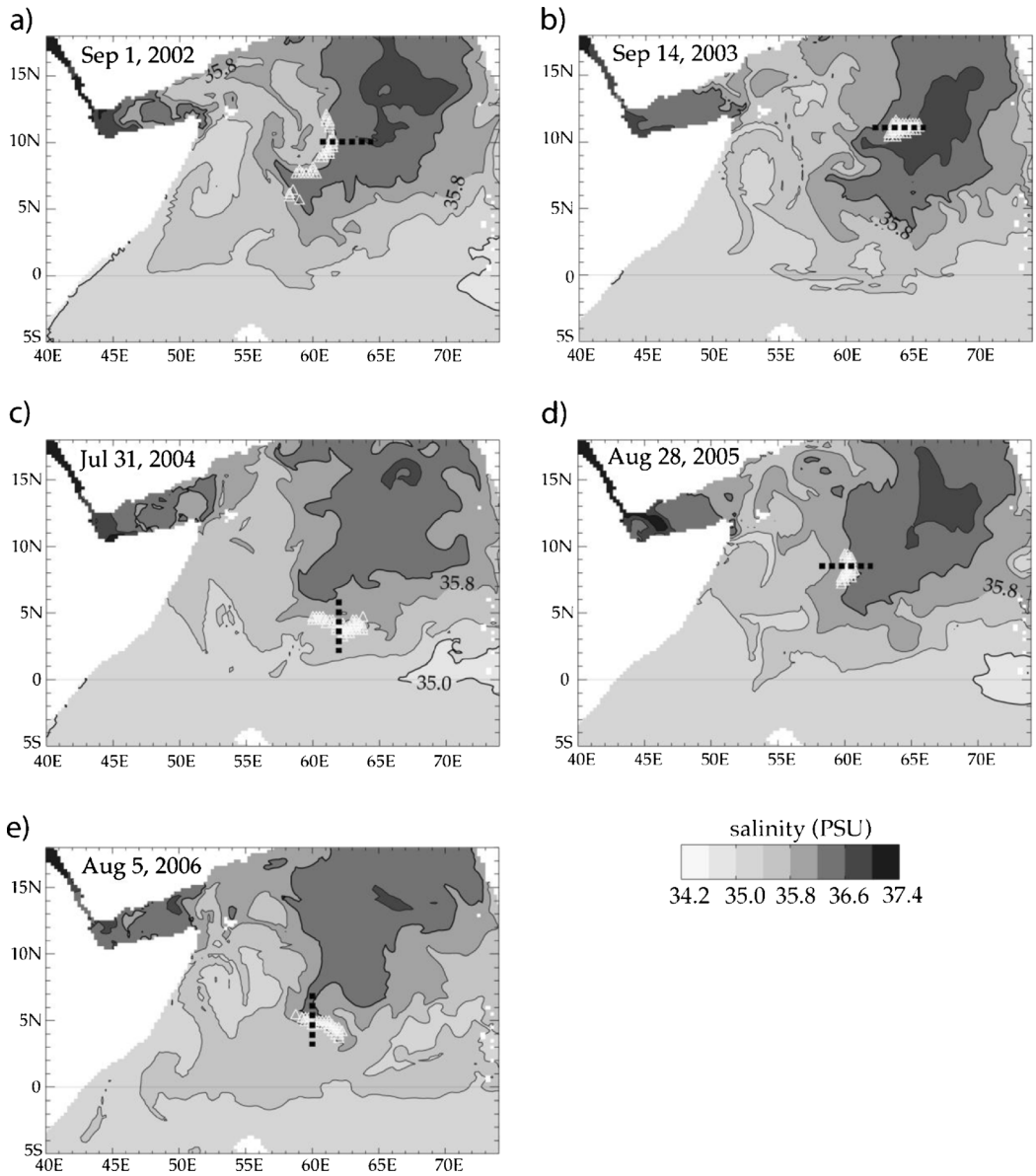

Fig. 5 Modeled salinity at 78 m depth on the same dates as for Fig. 4. *White triangles* show the locations where the BLT exceeds the threshold specified in Table 1. The *thick dashed* lines locate the sections presented in Fig. 6. Isocontours are every 0.4 psu

mechanism corresponds to the "tilting" defined by Cronin and McPhaden (2002), but with a slight difference: all (but one) batches of particles show unambiguous sign of a subduction in the period preceding the BL buildup. ASHSW flows southeastward (and downward), and finally gets blanketed locally by BBW to form the BL at the frontal zone. In a manner similar to Lagrangian tracing of the BL water mass, we also investigated the origin of the ML water overlying the BL for all the events, in the same way as Durand et al. (2007); we do not detail the results here for the sake of conciseness. We found that the ML water prominently originates from the western Arabian Sea (either in the Somali Current or further offshore in the interior Arabian Sea) and flows eastward before reaching the frontal area. Therefore, the BL formation process resembles the one evidenced in the frontal zone of the western equatorial Pacific Ocean by Vialard and Delecluse (1998) with a similar model. Here, however, the movement of the water mass whose

Table 1 Threshold in BLT chosen to define the maximum BLT area plotted for each year in Fig. 5. The number of model grid points passing the threshold criterion is also indicated

Year	2002	2003	2004	2005	2006
BLT threshold	80 m	60 m	75 m	80 m	80 m
Number of grid points	34	36	41	24	30

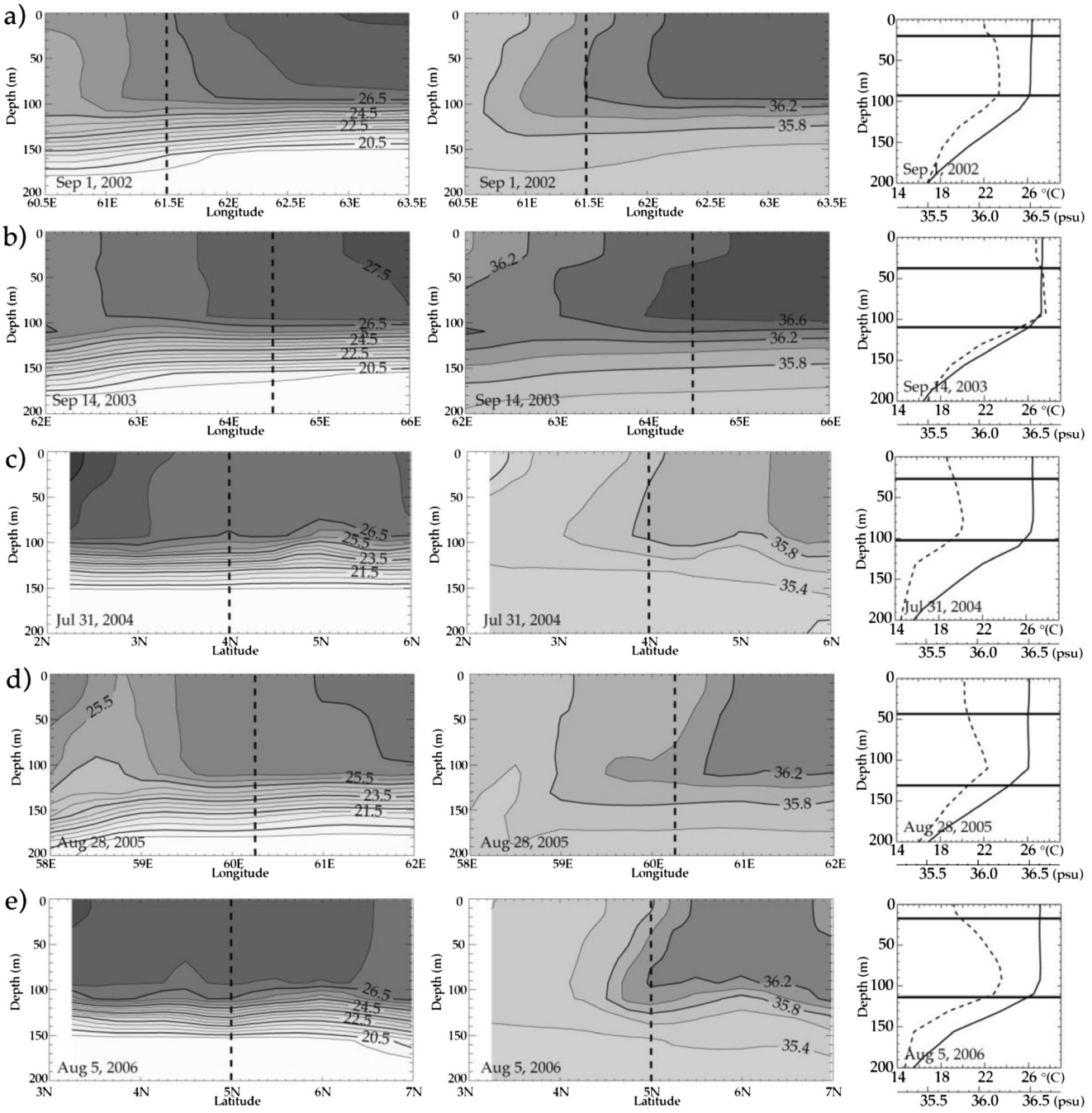

Fig. 6 *Left column*: vertical sections of modeled temperature along the sections shown in Fig. 5 and for the same five dates (panels **a** to **e**; years 2002 to 2006). The contour interval is 0.5 °C. *Middle column*: same as left column, but for salinity and with a 0.2 psu contour interval. *Right column*: temperature (*full line*) and salinity (*dashes*) profiles extracted at the position shown by the *vertical dashed lines* on the *left* and *middle columns*, located in the core of the BL. The *two horizontal lines* show the depth of the mixed layer (MLDρ) and the depth of the top of the thermocline (TTD, defined following the criteria mentioned in Section 2). The BL is thus seen as the layer comprised between these two lines

fate is the core of the BL occurs predominantly in a direction parallel to the salinity front, whereas the BL analysed by Vialard and Delecluse (1998) was formed by subduction in the cross-frontal direction. We applied the same Lagrangian analysis to the three thickest BL patterns simulated by the model each year, from 2002 to 2006 (thus amounting to 15 patterns; not shown). This extended diagnosis essentially confirms what is seen from the five major patterns thoroughly analysed: most of the BL patterns are formed by tilting through subduction of ASHSW below BBW, in a region of small horizontal extent centred on the salinity front. On a few occasions, the BL is formed by pure tilting mechanism, without any vertical migration of the water masses.

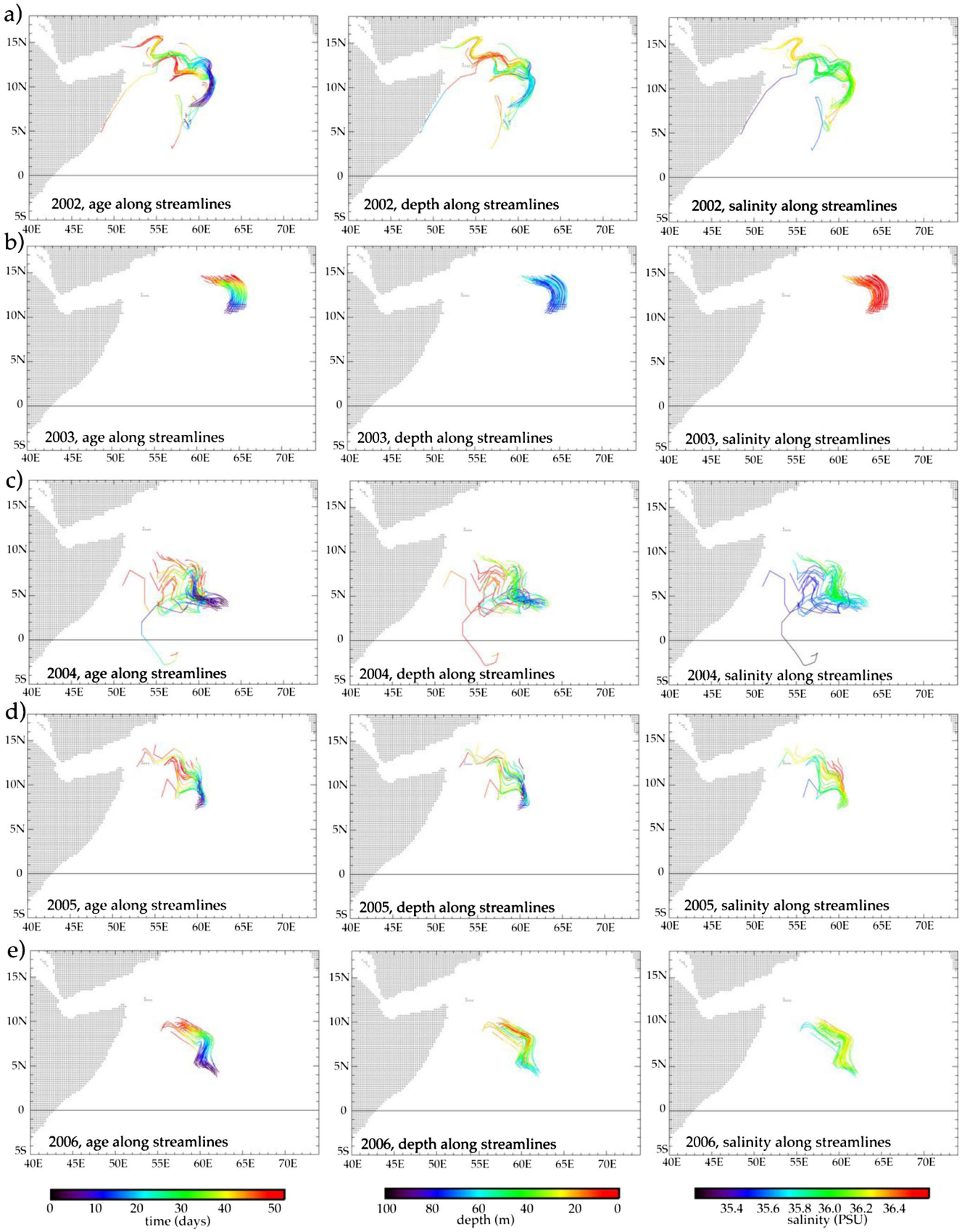
a)
2002, age along streamlines
2002, depth along streamlines
2002, salinity along streamlines
b)
2003, age along streamlines
2003, depth along streamlines
2003, salinity along streamlines
c)
2004, age along streamlines
2004, depth along streamlines
2004, salinity along streamlines
d)
2005, age along streamlines
2005, depth along streamlines
2005, salinity along streamlines
e)
2006, age along streamlines
2006, depth along streamlines
2006, salinity along streamlines
15N
10N
5N
0
5S
40E 45E 50E 55E 60E 65E 70E
0 10 20 30 40 50
time (days)
100 80 60 40 20 0
depth (m)
35.4 35.6 35.8 36.0 36.2 36.4
salinity (PSU)

◀ **Fig. 7** *Left column*: age of Lagrangian particles along model streamlines, during the 55-day-long backward integrations starting on the same dates as Fig. 5 (panels **a** to **e**: years 2002 to 2006). The fate of the Lagrangian particles (corresponding to day #0) are the thick BLT areas shown by the *white triangles* in Fig. 5. *Middle* and *right columns*: same as left column, for depth and salinity of the particles along streamlines, respectively

6 Discussion

Based on the available observations and on a general circulation model, we have shown that the BL in the Arabian Sea during summer monsoon has a small horizontal extent. It appears to be locked on the salinity front separating ASHSW and BBW. The model suggests that BL events take the form of elongated patterns, stretched along the salinity front, with typical length and width of a few hundreds km and of 100 km, respectively. This stretched shape can be explained by the stirring of the geostrophic current expected to flow along the front, as a response to the cross-frontal pressure gradient. Because of their spatio-temporal coverage, the available observations do not resolve the detailed structure of these patterns. As a consequence, the observed summer Arabian Sea BL appears as highly porous (with typical porosity of 50 %) at the space and time scales resolved for porosity computation (2°, 1 month). This corresponds to a space and lifetime of the BL of order 15 days and/or 100 km or less.

As such, our study contradicts the findings of RS03 and of T08, who reported a thick (20 m to over 40 m), large-scale BL throughout the central Arabian Sea during summer (July to September). The reason for this inconsistency is not straightforward, in particular since T08 used an observational dataset similar to ours. To try to find out an explanation for those differences in BLT amplitude and surface area (between the present study, M09, A12 on one hand and RS03 and T08 on the other hand), we perform some tests on the various methods used to obtain the final monthly BLT fields. We use the same initial dataset for our tests, consisting of all Argo profiles in the area between 2004 and 2012 (similar to the dataset used for Fig. 2, except that here we do not have Argo before 2004 nor CTD profiles). For the gridded climatology of T/S profiles we use the Roemmich and Gilson (2009) dataset over the same period (2004 to 2012), from which we simply obtain the T/S profiles annual monthly climatology by averaging the 9 years (note that our results are nearly identical if we use the interannual monthly grids of Roemmich and Gilson (2009) instead). We focus on the months of July and August when the peak of the BL occurs. Figure 8 shows the final maps of BLT for the 2 months, obtained through the three different types of methods used in the past and present studies: left column shows the resulting monthly maps for a method similar to RS03 and A12 (who used a 1 °C BLT criterion from climatological gridded T and S profiles), middle column shows the results for a method similar to T08 (who used a 1 °C BLT criterion from individual profiles and then performed a mapping through kriging), and right column shows the results of the same method similar to T08 except that we use a 0.2 °C criterion for BLT (as in the present study). For the central and right maps in Fig. 8, the mapping method we chose to get the BLT monthly state from individual values uses Data Interpolating Variational Analysis (DIVA; Troupin et al. 2012, with a covariance scale of 4°, and an error of 20 %). It is a method very close to optimal interpolation (Troupin et al. 2012). We also tested a direct ordinary kriging as well as a method identical to de Boyer Montégut et al. (2004) and we get very similar results (with even slightly less extended spatial patterns).

We can draw two conclusions from Fig. 8. First, for a given BLT criterion (1.0 °C, left and middle columns), computing BLT either from individual T/S profiles or from climatological T/S grids has not such a strong influence. Resulting patterns are similar, with a slightly reduced amplitude for the case of BLT based on climatological T/S grids. A reverse effect, i.e., a little increase, is seen for the 0.2 °C criterion (not shown), so it appears that the bias effect that was discussed for the computation of ML depth by de Boyer Montégut et al. (2004) is somehow compensated when dealing with a difference of ML depths. Second, for a given computation method (BLT based on individual T/S profiles, middle and right columns), the influence of the criterion on the amplitude of the BLT pattern is very minor and does not appear systematic. In July, the 0.2 °C criterion yields deeper BLTs, while it gives shallower BLTs in August. This point will be further discussed in the next paragraph. In both months, the 0.2 °C criterion yields a BL area of greater extent.

By using either a 0.2 °C vs. a 1 °C criterion for the BLT computation, we do not pick exactly the same water layer (one lies below the other and thus is not exactly associated with a BL of identical characteristics, especially its timescales). However, on average, the thickness of the layer is not affected by the choice of the criterion, at least for our study area. Figure 9 provides an example of profiles where the BLT obtained through a 0.2 °C criterion can be either larger or smaller than the BLT obtained through a 1 °C criterion. This is consistent with what is shown in Fig. 8. Note that this result might not hold in other areas like the mid or high latitudes where the subsurface stratification is much less marked than in the tropics (leading to some possible inaccuracies with the 1 °C criterion).

At last, to further clarify the issue of the BL amplitude differences, we computed the "revisited-BLT" (in the sense of M09). It is defined as the median of all significant BLT in each grid cell, calculated after discarding weak BL patterns. It thus represents the mean state of BLT when and where a significant BL occurs in the grid cell, and not the mean state of the BLT over the whole month and area of the grid cell. We obtained a value of 20 m to 40 m for summer BLT in the SCAS (not

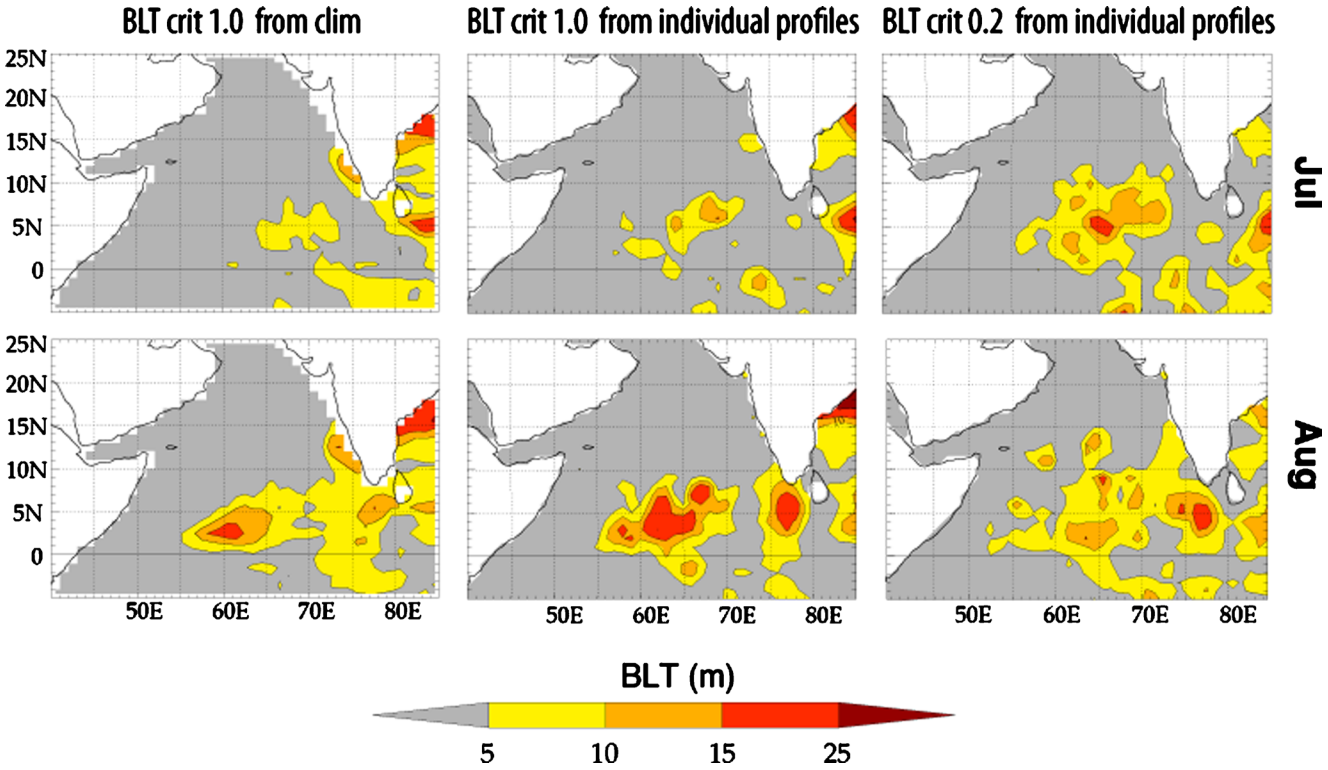

Fig. 8 Maps of the climatological state of barrier layer thickness (*BLT*) for the months of July (*top panels*) and August (*bottom panels*), obtained from three different methods: estimation of BLT with a 1 °C criterion from climatological gridded T/S profiles (*left column*), estimation of BLT with a 1 °C criterion from individual profiles and gridding (*middle column*), estimation of BLT with a 0.2 °C criterion from individual profiles and gridding (*right column*), spatial resolution is 1°×1°, see text for details

shown), in line with RS03 and T08 estimates. However, this revisited BLT is meaningless if considered independently from its associated porosity value. It does not represent the "barrier" effect of the BL in the studied area, but rather the BLT during effective events. Also it is not the method that T08 or RS03 described to have used.

The conclusion of this sensitivity test stands in line with the study of A12 who reported a thin BLT of 10–15 m (using a

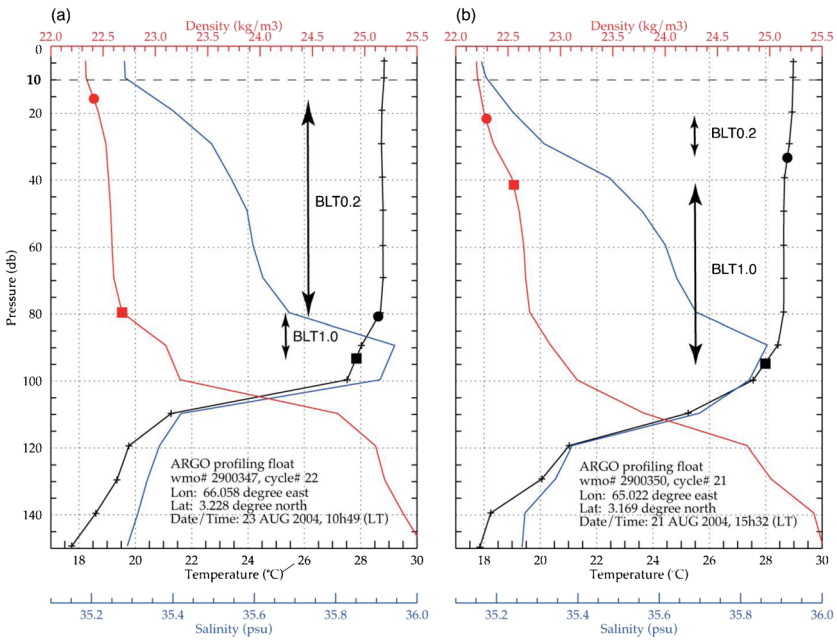

Fig. 9 **a** Same as Fig. 1, with the *black square* indicating the depth where the temperature is 1.0 °C colder than at 10 m (T10), and the *red square* indicating the depth of the corresponding density increase. The barrier layer thickness in the sense T10-1.0 °C, named BLT1.0, is defined as the depth difference between the *black* and *red squares*. Here, BLT1.0=14 m, i.e., significantly less than BLT0.2 (65 m). **b** Same as **a**, for another ARGO profile (float # 2900350), in the same area and in the same period (the two stations are separated by 2 days and 115 km). For profile **b**, we have BLT0.2=12.6 m and BLT1.0=53.5 m (i.e., significantly more than BLT0.2)

1 °C criterion) during summer in the SCAS, as well as with M09 who estimated a BLT of 10–20 m (using a 0.2 °C criterion). Just like in these studies, our climatological BLT estimate (both observed, Fig. 8 right column, and modeled, Fig. 2c) is quite thin (inferior to 25 m) in the SCAS during summer, because of the year-to-year variability of the location of the isolated events of thick BL discussed above. The amplitude of the climatological BL reported by RS03 and T08 exceeds our estimates by a factor of about 2 (extended BLT over 40 m in August for T08). We can conclude that this cannot be explained by the method used (neither the BLT criterion, nor the use of individual T/S profiles vs. climatological T/S grids) as we showed above for a given dataset. Thus it appears that such a thick BL is doubtful, and we cannot provide any explanation about the reason for this inconsistency.

In all cases, using objective mapping as a method to fit the basic hydrographic data (either T/S profiles, or BLT individual values), smoothens the distributions to a significant degree. In both our case and T08 study, this creates relatively extended spatial patterns of BL. This hides the details, in particular the role of the mesoscale fronts evidenced in this work. This may explain why T08 describe the BL formation as a large-scale process. In the present study, both the use of the porosity index and of an OGCM allowed us to infer the short space and time scales of the BL events.

Our circulation model showed that the formation process of summer BL in the SCAS is essentially the tilting mechanism defined by Cronin and McPhaden (2002), though with a distinctive feature: most of the time, ASHSW gets downwelled at the salinity front before flowing beneath BBW and building up the BL. As such, the formation mechanism we propose is similar to the one suggested by T08, although our model shows that this layered structure is of small spatial and temporal extent in the close vicinity of the frontal area, and is not seen at large scale as they suggested. Interestingly, our study evidences a meso-scale BL formation process, capable of generating extremely thick BL patterns without any external freshwater supply.

That last point holds effectively for the major BL events we have chosen in the model to illustrate the role of fronts in their formation. However, our area of study (especially the box in Fig. 2), while being out of the main monsoon precipitation zone, may experience some episodic rainfall events. From June to September, climatological monthly values are around 5 mm/day in that box, and daily precipitation of about 50 mm can be observed from TRMM dataset (3b42_v6 product), especially around the southern and eastern edge of the box, while north and west are very rarely exposed to precipitations. It has been shown that BL can form and last for a day or more (depending on the wind conditions) with, for example, rainfall events of about 60 mm in 2 h (Price 1979; You 1998), which are not represented by our model. As a matter of fact, while the frontal mechanism certainly accounts for the majority of thick BL events in SCAS, we cannot totally exclude that some rainfall mechanism may also happen locally at some occasions for not more than a few days, especially around southern and eastern edge of our box of study.

Because of its limited spatial and temporal scales, the summertime Arabian Sea BL probably plays a negligible climatic role: globally, at large scale, the Arabian Sea can be considered as essentially BL-free throughout the summer monsoon.

The BL formation mechanism we invoke implies an active role of the mesoscale circulation in the frontal area. However, one has to keep in mind that our model is eddy-permitting only, and in particular does not represent the sub-mesoscale circulation nor the baroclinic instabilities likely to develop in the mixed-layer in the frontal area. It will be necessary to revisit our conclusions with a fully eddy-resolving model of the Arabian Sea, when such high-resolution systems become available.

Acknowledgements This study was funded by IRD, IFREMER, Mercator Océan and CNRS. Support from these institutions is gratefully acknowledged. We are indebted to the people who set up the International ARGO Project and made the ARGO dataset freely available. The model simulations were performed on a SGI computer. We made extensive use of the SAXO software (http://forge.ipsl.jussieu.fr/saxo) developed by Sébastien Masson for plotting. We appreciated constructive comments by Gurvan Madec.

References

Agarwal N et al (2012) Argo observations of barrier layer in the tropical Indian Ocean. J Adv Space Res. doi:10.1016/j.asr.2012.05.021

Antonov JI, Locarnini RA, Boyer TP, Mishonov AV, Garcia HE (2006) In: Levitus S (ed) World ocean atlas 2005, Volume 2: Salinity. NOAA Atlas NESDIS 62, U.S. Government Printing Office, Washington, D.C, 182 pp

Arakawa A (1966) Computational design for long term numerical integration of the equations of fluid motion, two dimensional incompressible flow. Part I. J Comput Phys I:119–149

Blanke B, Delecluse P (1993) Variability of the tropical Atlantic Ocean simulated by a general circulation model with two different mixed layer physics. J Phys Oceanogr 23:1363–1388

Blanke B, Raynaud S (1997) Kinematics of the Pacific Equatorial Undercurrent: an Eulerian and Lagrangian approach for GCM results. J Phys Oceanogr 27:1038–1053

Blanke B, Arhan M, Madec G, Roche S (1999) Warm water paths in the equatorial Atlantic as diagnosed with a general circulation model. J Phys Oceanogr 29:2753–2768

Boyer TP, Antonov JI, Baranova OK, Garcia HE, Johnson DR, Locarnini RA, Mishonov AV, O'Brien TD, Seidov D, Smolyar IV, Zweng MM (2009) World ocean database 2009. In: Levitus S (ed) NOAA atlas NESDIS 66. U.S. Gov. Printing Office, Wash., D.C., pp 216, DVDs

Chatterjee A, Shankar D, Shenoi SSC, Reddy GV, Michael GS, Ravichandran M, Gopalakrishna VV, Rama Rao EP, Udaya Bhaskar TVS, Sanjeevan VN (2012) A new atlas of temperature and salinity for the North Indian Ocean. J Earth Syst Sci 121(3):559–593

Cronin MF, McPhaden MJ (2002) Barrier layer formation during westerly wind bursts. J Geophys Res 107(C12):8020. doi:10.1029/2001JC001171

de Boyer Montégut C, Madec G, Fischer AS, Lazar A, Iudicone D (2004) Mixed layer depth over the global ocean: an examination of profile data and a profile-based climatology. J Geophys Res 109, C12003. doi:10.1029/2004JC002378

de Boyer Montégut C, Mignot J, Lazar A, Cravatte S (2007a) Control of salinity on the mixed layer depth in the world ocean: 1. General description. J Geophys Res 112, C06011. doi:10.1029/2006JC003953

de Boyer Montégut C, Vialard J, Shenoi SSC, Shankar D, Durand F, Ethé C, Madec G (2007b) Simulated seasonal and interannual variability of mixed layer heat budget in the north Indian Ocean. J Clim 20: 3249–3268. doi:10.1175/JCLI4148.1

Durand F, Shankar D, de Boyer Montégut C, Shenoi SSC, Blanke B, Madec G (2007) Modeling the barrier-layer formation in the South-Eastern Arabian Sea. J Clim 20(10):2109–2120. doi:10.1175/JCLI4112.1

Durand F, Alory G, Dussin R, Reul N (2013) SMOS reveals the signature of Indian Ocean Dipole events. Ocean Dyn. doi:10.1007/s10236-013-0660-y

Esenkov OE, Olson DB, Bleck R (2003) A study of the circulation and salinity budget of the Arabian Sea with an isopycnic coordinate ocean model. Deep-Sea Res II 50:2091–2110

Goosse H, Campin JM, Deleersnijder E, Fichefet T, Mathieu PP, Maqueda AAM, Tartinville B (2001) Description of the CLIO model version 3.0. Institut d'Astronomie et de Géophysique Georges Lemaitre, Catholic University of Louvain, Belgium

Hoyos CD, Webster PJ (2007) The role of intraseasonal variability in the nature of Asian monsoon precipitation. J Clim 20(17):4402–4424

Locarnini RA, Mishonov AV, Antonov JI, Boyer TP, Garcia HE (2006) In: Levitus S (ed) World ocean atlas 2005, Volume 1: Temperature. NOAA Atlas NESDIS 61, U.S. Government Printing Office, Washington, D.C, 182 pp

Lukas R, Lindstrom E (1991) The mixed layer of the western equatorial Pacific Ocean. J Geophys Res 96(Suppl):3343–3358

Madec G (2008) NEMO reference manual, ocean dynamics component. Note du pôle de modélisation, IPSL France N°27 ISSN N°1288-1619

Maes C, Picaut J, Belamari S (2005) Importance of salinity barrier layer for the buildup of El Niño. J Clim 18:104–118

Masson S, Luo JJ, Madec G, Vialard J, Durand F, Gualdi S, Guilyardi E, Behera S, Delecluse P, Navarra A, Yamagata T (2005) Impact of barrier layer on winter–spring variability of the South-Eastern Arabian Sea. Geophys Res Lett 32, L07703. doi:10.1029/2004GL021980

Mignot J, de Boyer Montégut C, Lazar A, Cravatte S (2007) Control of salinity on the mixed layer depth in the world ocean: 2. Tropical areas. J Geophys Res 112, C10010. doi:10.1029/2006JC003954

Mignot J, de Boyer Montégut C, Tomczak M (2009) On the porosity of barrier layers. Ocean Sci 5:379–387. doi:10.5194/os-5-379-2009

Prasad TG, Ikeda M (2002) A numerical study of the seasonal variability of Arabian Sea high-salinity water. J Geophys Res 107(C11):3197. doi:10.1029/2001JC001139

Prasanna Kumar S, Prasad TG (1999) Formation and spreading of Arabian Sea high salinity water mass. J Geophys Res 104(C1):1455–1464

Price JF (1979) Observations of a rain-formed mixed layer. J Phys Oceanogr 9:643–649

Rao RR, Sivakumar R (2003) Seasonal variability of sea surface salinity and salt budget of the mixed layer of the north Indian Ocean. J Geophys Res 108:3009. doi:10.1029/2001JC000907

Roemmich D, Gilson J (2009) The 2004–2008 mean and annual cycle of temperature, salinity, and steric height in the global ocean from the Argo Program. Progr Oceanogr 82:81–100

Thadathil P, Thoppil P, Rao RR, Muraleedharan PM, Somayaju YK, Gopalakrishna VV, Murthugudde R, Reddy GV, Revichandran C (2008) Seasonal variability of the observed barrier layer in the Arabian Sea. J Phys Oceanogr 38:624–638

Tomczak M (1999) Some historical, theoretical and applied aspects of quantitative water mass analysis. J Mar Res 57:275–303

Troupin C, Barth A, Sirjacobs D, Ouberdous M, Brankart J-M, Brasseur P, Rixen M, Alvera Azcarate A, Belounis M, Capet A, Lenartz F, Toussaint M-E, Beckers J-M (2012) Generation of analysis and consistent error fields using the Data Interpolating Variational Analysis (Diva). Ocean Model 52–53:90–101

Vialard J, Delecluse P (1998) An OGCM study for the TOGA decade: part II. Barrier layer formation and variability. J Phys Oceanogr 28: 1089–1106

Wirth A, Willebrand J, Schott F (2002) Variability of the Great Whirl from observations and models. Deep-Sea Res II 49: 1279–1295

You Y (1998) Rain-formed barrier layer of the western equatorial Pacific warmpool: a case study. J Geophys Res 103(C3):5361–5378